FATIGUE AND FRACTURE MECHANICS OF A WROUGHT Ni-BASE ALLOY

R.B.Scarlin*, K.N.Melton* and W.Hoffelner+

The creep and fatigue properties of the Ni-base alloy Nimonic 901 have been investigated. Both conventional methods using cylindrical specimens and fracture mechanics techniques using precracked testpieces have been employed to obtain a fuller understanding of the behaviour of the material also with respect to defect tolerances. Creep and fatigue tests have been performed at various temperatures and mean stresses and the results correlated with the modes of fracture observed. Examination of the test specimens has shown a) for cylindrical specimens, the role of microstructural features in the initiation of cracks and b) for the fracture mechanics specimens, the mechanism of interaction of the propagating cracks with various microstructural features.

INTRODUCTION

Materials for applications in gas turbines are required to withstand exacting operating conditions. They must exhibit good strength to permit their use in lightweight designs and high creep resistance so that operating temperatures can be raised to increase thermal efficiency, while maintaining a long service life of the equipment. In addition they need a high resistance to fatigue loading including both high cycle fatigue from vibration or rotating bending of the rotor and low cycle fatigue arising predominantly from the steep thermal gradients occurring during rapid start-up and shut-down of the machine.

Since the temperature of the material can vary between sub-zero for the start-up of a turbine located in the open-air to the maximum gas temperature during operation at full load it is clear that a knowledge of the temperature dependence of these fatigue and creep properties is of paramount importance. For a complete evaluation of the integrity, for example, of a rotor it is necessary to perform both fracture mechanics tests using precracked specimens and conventional tests with cylindrical specimens which are either creep or fatigue loaded under different conditions. It is important to consider crack initiation and propagation both for slow crack growth under creep or fatigue and for fast fracture under overload conditions.

TESTING MATERIAL

Since previous tests (1) on the alloy Nimonic 901 have been performed on specimens taken from relatively small test blocks it was decided to employ a forging of a size suitable for use in the manufacture of a gas turbine rotor in the present work. For this reason all specimens were machined from a disc of diameter

* Brown Boveri Central Laboratory, Baden, Switzerland
+ Brown Boveri Research Centre, Dättwil, Switzerland

970 mm and length 230 mm which had had the normal heat treatment of 3 hrs 1090°C, water quench, 2 hrs 775°C, air cool and 24 hrs 700°C air cool. The chemical analysis is given in Table 1. A check of the uniformity of the mechanical properties was performed, prior to beginning the test programme, by carrying out tensile and Charpy tests on specimens taken from the rim and centre regions (Specimen direction tangential). It is shown in Table 2 that there is no significant difference between the properties at the centre and rim of the forging despite the somewhat larger concentration in the centre region of (Nb, Mo) (C, N) type particles (electron microprobe identification).

TESTING PROGRAME

Cylindrical Specimens

Creep testing. Creep tests were carried out in the temperature range of 400 to 550°C using cylindrical specimens which had been machined from the centre of the forging such as to be stressed in a direction radial to the centreline. The specimen contains separate smooth and notched sections each of diameter approx. 8 mm so that the nominal stress of both parts is identical (see Fig. 1). The elastic stress concentration factor of the notch, calculated according to Neuber (2), is 3.

Strain measurements were made periodically using a travelling microscope after removing the specimen from the furnace and allowing it to cool. The measurements indicated normal behaviour in the primary and secondary ranges with a prolonged secondary region exhibiting a constant creep rate, but a rather abrupt transition to a brief region of tertiary creep prior to failure. The creep rupture curves for the temperatures of 400, 500 and 550°C are shown in Fig. 1. Comparison of the curves with the values of the tensile strength determined at the same temperature shows for example that very little creep occurs at 400°C. A creep specimen loaded at a stress 2 % below the tensile strength is still intact after 13'000 hours test duration. At 500 and 550°C there is an increase in gradient of the creep rupture curves. Specimen failures have been obtained at times approaching 10'000 hours.

After the first failure of the specimen, which always occurred in the parallel test section, testing of the notched portion was continued at the same nominal stress i.e. the material does not exhibit notch sensitivity at testing times upto 13'000 hours. Figure 2 shows the reduction in the creep strain to failure at longer testing times and higher temperatures by plotting the values

TABLE 1 - Chemical Composition (wt.%).

C	Cr	Mo	Ti	Fe	P	S	Co	Ni
0.08	12.7	6.2	2.8	37.4	0.004	0.003	0.9	Bal.

TABLE 2 - Mechanical Properties (Duplicated measurements).

Specimen location	0.2% Proof strength MPa	Tensile strength MPa	Elongation to failure %	Reduction of area %	Charpy impact energy J
Rim	868/908	1134/1131	20/17	21/19	31/44
Centre	908/939	1072/1169	14/22	15/24	31/43

against a Larson-Miller parameter (3). Although there is considerable scatter in the fracture strain values and a progressive reduction in the measured values, they do not fall below 5 % even after the longest tests.

Microstructural studies were performed using optical and scanning electron microscopy techniques to elucidate the mechanism of this loss of creep ductility. Optical sections taken from the gauge length and unstressed head section of creep specimens tested at different temperatures and for different durations indicate that extensive precipitation reactions occur within the grains along slip bands. The precipitates are barely visible in the gauge length of creep samples which fail after 800 hrs at 500°C but are larger after 100 hr tests at 550°C. An increase to approaching 10'000 hrs at 550°C indicates copious precipitation on slip bands in the gauge section, Fig. 3, but practically no precipitation in the sample head. The precipitates can be tentatively identified as η phase since it has been stated in a number of publications (4, 5) that for ratios Ti:Al greater than 5 the stable precipitate is η phase with the composition Ni_3Ti and a hexagonal structure. Although the reaction $\gamma' \rightarrow \eta$ normally only occurs at temperatures considerably in excess of the 550°C employed here, it has been shown that the reaction is accelerated in the alloy A 286, which has a broadly similar composition and structure to that of Nim 901, when the specimen is subjected to a simultaneous creep deformation (5).

As the precipitation reaction proceeds there is an increasing prevalence of large transgranular facets on the mixed mode trans/intergranular fracture surface where the creep crack appears to heave propagated along planes of such precipitates (Fig. 4 a, b). Further tests have indicated that creep failure is purely intergranular at 400°C but predominantly transgranular above 550°C.

Low cycle fatigue testing. Specimens for low cycle fatigue testing were machined from the rim of the forging in such a direction that loading was radial to the centre line. The tests were performed on smooth specimens of diameter ca. 16 mm under longitudinal strain control in a servo-hydraulic testing machine. A triangular strain wave was employed with a strain rate of 10^{-3} per second for both the room temperature and 500°C tests. Failure of the specimens was defined at a load drop of 5 % compared to the load level at one half of the number of cycles to the point where an inflection was noted in the compressive part of the hysteresis cycle, indicating the presence of a crack.

Figure 5 shows the results obtained at room temperature and 500°C. They agree well with data available in the literature (6, 7). It is apparent that, at the same total strain amplitude, specimens tested at 500°C exhibit around 40 % of the lifetime measured at room temperature. This reduction in total strain range with increase in temperature for a certain number of cycles to failure in the low cycle fatigue range of about 25 % is similar to that previously reported (8) between the fatigue limit values for this heat of Nimonic 901 at > 10^8 cycles to failure, indicating at least qualitatively a similarity in the effect of testing temperature in the low cycle and high cycle ranges.

The following observations can be made:

a) there is no clear effect of surface quality on the room temperature lifetime (the turned specimens had either the normal centre line average surface roughness of 0.8 µm or an increased roughness of 12 µm)
b) hold times do not cause a reduction of the lifetime at 500°C. Hold times of 30 minutes in tension and/or compression had no significant effect in the range upto about 700 cycles consistent with the observed high creep strength of the material at this temperature and the absence of any measureable stress relaxation during the hold time. Microstructural damage during these hold times

must be negligible. Only slight traces of the start of precipitation on slip bands was visible after the longest hold time tests at 500°C. Scanning electron microscopy of the fracture surfaces indicates that both at room and elevated temperature cracks nucleate at the specimen surface and propagate in a mixed mode exhibiting a facetted type of transgranular cracking along with regions containing ductile dimples. Figure 6 shows a typical example for the lower temperature. The incorporation of hold times at 500°C affected neither the fracture surface morphology nor the appearance of the striations.

High cycle fatigue specimens tested at both room temperature and 500°C (8) indicate that cracking initiates at carbides intersecting the surface and propagates initially through the first few grains in a crystallographic Stage I mode. Subsequent failure occurs normal to the applied stress also exhibiting a mixed mode appearance.

Fracture mechanics testing

Fracture toughness. Specimens machined from the centre, rim and midradius of the forging have been used for the determination of the fracture toughness in the temperature range -40 to 500°C. The compact tension specimens of thickness 25 mm were loaded in a direction radial to the axis of the forging. The elastic-plastic fracture toughness (J_{IC}) was determined using the partial unloading technique in which strain controlled tests were performed in a servohydraulic testing machine at a rate of 0.01 mm per second at the loading line. Partial unloading was carried out manually to determine the specimen compliances and thereby the crack length. The crack growth resistance curve (J versus Δa) was then determined using the method outlined in the ASTM proposal and the critical value J_{IC} was taken as the intersection of this line with the theoretical blunting line:

$$J = 2\sigma_F \Delta a$$

where σ_F, the flow stress, is taken as the mean of the yield strength and ultimate tensile strength at the appropriate testing temperature.

As an example Fig. 7 shows the results of 6 tests made at 500°C on specimens from the mid-radius. As indicated in the diagram two of the specimens were tested using the partial unloading technique whereby the final crack length (extended by over 2 mm) was marked using heat tinting. Of the remaining four specimens which were heat tinted, only two showed measureable crack growth (0.1 and 3.0 mm respectively).

Upper and lower bound lines have been extrapolated back to intersect the blunting line giving a critical toughness J_{IC} of 84 ± 13 N/mm. This value is plotted along with the measurments made at lower temperatures, Fig. 8. There is considerable scatter in J_{IC} values particularly at the lower testing temperatures but no consistent difference between results from the centre and rim of the forging. This is also consistent with the observed Charpy impact energies which show a difference between measurements from nominally identical positions of about 50 % but no clear difference between the centre and rim regions (Table 2). The fracture toughnes does not increase with increasing testing temperature as is the case for ferritic steels. In fact a lower bound curve below these measurements would indicate that the fracture toughness is independent of location within the forging and test temperature.

A SEM investigation performed to elucidate the reasons for the observed differences in fracture toughness indicated that specimens tested both at the lowest and highest temperatures exhibit mixed mode trans-intergranular frac-

ture regardless of whether high or low toughness values had been measured. Fine dimples, which were observed on the ductile areas of the fracture surfaces, were more prevalent at the highest testing temperature. The most significant difference between the fracture surfaces of the specimen showing high toughness and that showing low toughness at -40°C lies in the greater roughness of the fracture toughness in the former case. In the high toughness specimen (Fig. 9a) the fracture path appears to deviate around the prior dendrite boundaries where many cracked carbides are visible producing an increase in the fracture surface area and work of fracture. In contrast the low-toughness specimen shows a much flatter fracture (Fig. 9b).

Fatigue crack growth

Fatigue crack growth rates were measured in air as a function of the cyclic stress intensity range ΔK at RT, 300°C and 500°C at two different R-values (R = 0.1 and R = 0.5). The results are shown in Figures 10 and 11. At both R-values almost no difference exists between 300°C and RT in the Paris-region where the curves indicate mean growth rates. However, at 500°C a slight increase in crack growth rates and a small change in slope could be found. The region of very high ΔK was not investigated thoroughly because of the small thickness of the DCB-samples used (10 mm). In the threshold region where the curves indicate lower bounds, two facts are obvious. At room temperature a high amount of scatter could be found and at 500°C a very pronounced drop to a threshold value is apparent. The first observation is probably due to pronounced crystallographic crack growth leading to crack branching and inhomogeneously growing cracks. The second observation can be interpreted as an environmental effect. As it also occurs at R = 0.5 it can not simply be explained as a crack closure effect due to an oxide layer. Also other crack arresting effects such as blunting of the crack tip as a result of oxidation causing dissolution of precipitates and inducing weakening of the material at the crack tip play an important role. Further experiments in vacuum will be performed in order to clarify this point.

Creep crack growth

At 500°C and 600°C creep crack growth rates were studied as a function of the stress intensity factor, K. For these experiments 25 mm thick DCB-samples fatigue precracked at RT were used. For the determination of the creep crack growth rates the specimens were broken after certain testing times. The crack growth rates were determined from the measured length of the creep crack and the test time. From the results shown in Fig. 12 it follows that the creep crack growth curves can be well represented by a power law with almost temperature-independent exponent. A correlation of these exponents with the creep exponents of smooth samples was not as successful as in another investigation of other nickel-base alloys (9). In our case, the exponents of the creep crack growth laws were about 4 whereas the exponents in Norton's law were determined to be about 10 at 600°C and much higher at 500°C. It should also be mentioned that in the investigated range no signs of a threshold stress intensity for creep crack growth were found.

In Figure 13 we have attempted to combine creep and fatigue crack growth data on a crack growth - per cycle basis. A trapezoidal load wave shape was assumed with different hold times as also shown in Fig. 13. Creep crack growth was assumed to take place during the hold time whereas fatigue crack growth was assumed to occur during the unloading-loading period. Assuming further a linear summation of creep crack growth and fatigue crack growth we can see that upto half an hour hold time no significant creep crack growth should occur under these loading conditions in the Paris-region. In the threshold region however creep could become important, providing no threshold for creep crack

growth exists, which has not as yet been demonstrated.

For dwell times in excess of 5 hours the creep crack growth becomes important over the whole ΔK-regime. At 600°C fatigue crack growth rates are not expected to be much higher than those measured at 500°C. However, creep crack growth rates at 600°C have been shown previously to exceed the growth rates at 500°C by almost 2 orders of magnitude so that even 3 minutes hold times would become significant.

CONCLUSIONS

The present investigation of the properties of this Nimonic 901 forging has demonstrated the suitability of most of its properties for applications in a gas turbine. Good creep and low cycle fatigue properties are exhibited upto temperatures of at least 500°C although precipitation of a needle-like phase (probably η phase) appears to reduce creep ductility at longer testing times. Significant acceleration of fatigue crack propagation rates only appears above 300°C whereas creep crack growth rates remain low upto 500°C so that a significant increase in fatigue cracking rates due to hold times could only be expected at long times of operation at peak temperature. Fracture toughness values do not appear to increase with increasing temperature. They are only half as high as those of normal steels at operating temperatures.

ACKNOWLEDGEMENTS

The authors would like to express their thanks to the technicians in the central laboratory and research centre for their skilled assistance. The work was carried out within the framework of the COST-50 Round 3 cooperation and was financed in part by the Swiss Federal Government.

REFERENCES

1. McColvin, G.M., 1978, Proceedings of Conference on "High Temperature Alloys for Gas Turbines", Ed. Coutsouradis et al. Applied Science Publishers, London.

2. Neuber, H., 1959, "Kerbspannungslehre", Springer, Berlin.

3. Larson, F.R., and Miller, J., 1952, Trans. ASME 74, 765.

4. Betteridger, W., and Heslop, J., 1974, "The Nimonic Alloys", Edward Arnold, London.

5. Gulden, D., 1979, "Interaction of dislocations with precipitates", Diploma thesis, University of Erlangen, Department of Materials (in German).

6. Postans, P.J., and Jeal, R.H., 1978, Proceedings of Conference on "Forging and Properties of Aerospace Materials", The Metals Society, London.

7. Führing, H., 1979, Proceedings of Conference on "Low Cycle Fatigue Strength and Elasto-Plastic Behaviour of Materials", Deutscher Verband für Materialprüfung, Berlin.

8. Melton, K.N., Scarlin, R.B., and Hoffelner, W., 1982, to be published in Conference Proceedings of "High Temperature Alloys for Gas Turbines", Liége, Oct. 1982.

9. Floreen, S., 1975, Met. Trans 6A, pp. 1741-1749.

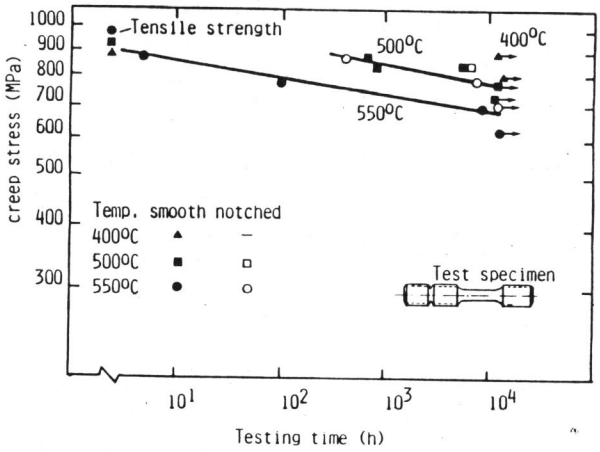

Figure 1 Creep rupture curves showing time to fracture of smooth and notched specimens at 400, 500 and 550°C.

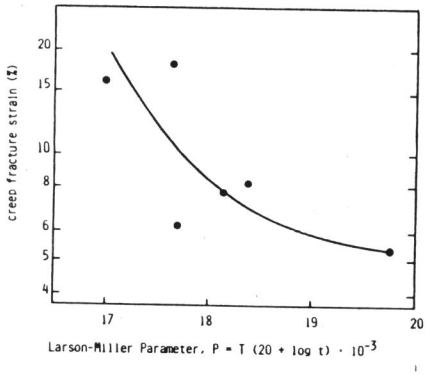

Figure 2 Reduction of creep strain to failure as a function of the Larson-Miller parameter.

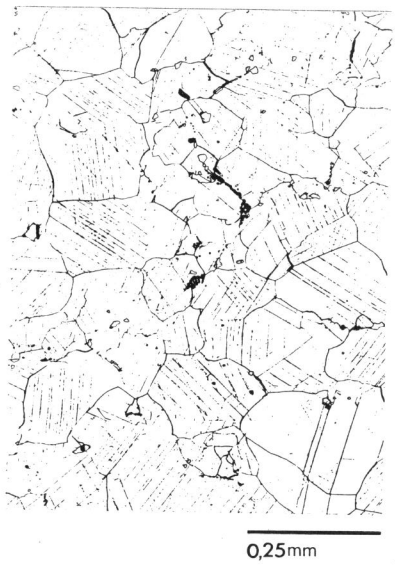

Figure 3 Optical micrograph showing precipitation on slip bands after creep testing to failure after 9400 hours at 550°C.

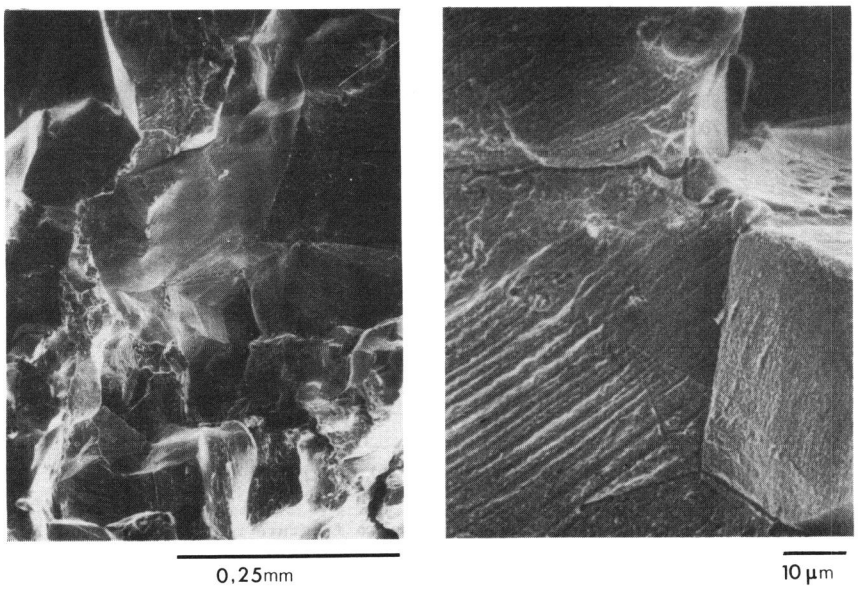

Figure 4 Mixed mode failure of creep specimen after 9400 hrs at 550°C. Crack has propagated along planes of precipitates.

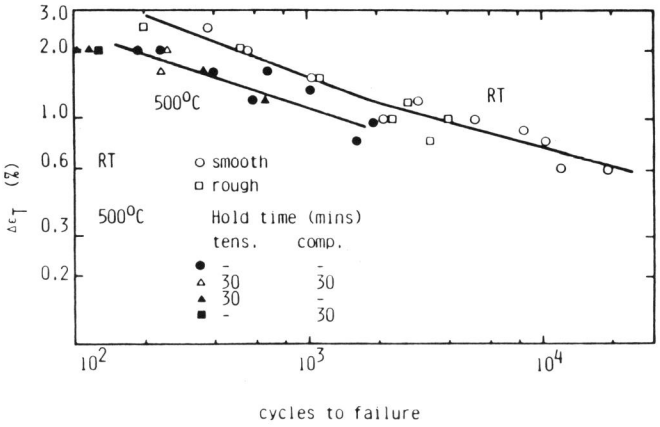

Figure 5 Low cycle fatigue lifetime curves at RT for smooth and rough specimen surfaces and at 500°C with and without hold times.

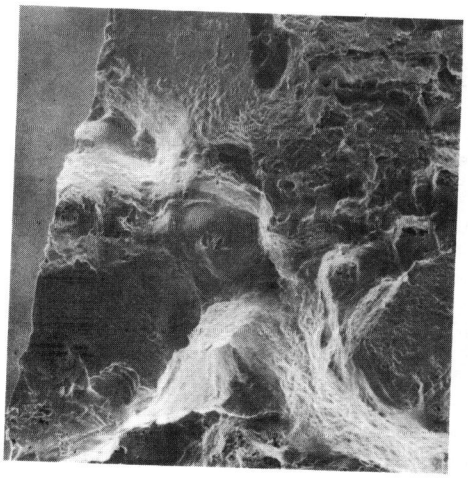

Figure 6 Facetted predominantly transganular low cycle fatigue cracking in a specimen tested at ambient temperature.

Figure 7 J-Integral crack growth resistance curve for Nim 901 at 500°C (6 specimens).

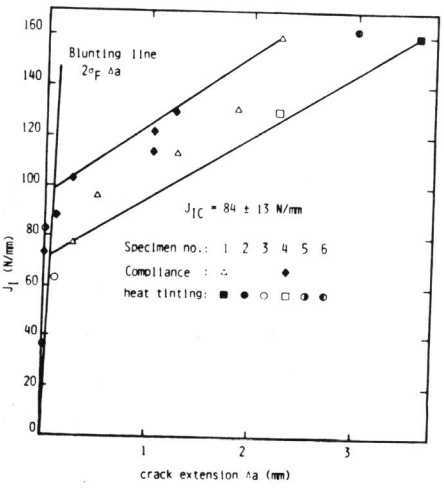

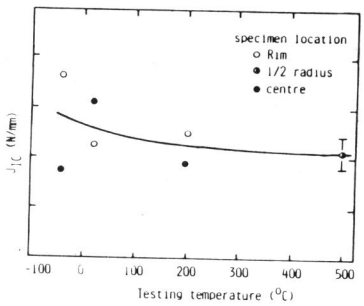

Figure 8 Depencence of critical value of J-Integral on testing temperature for specimens from various locations in the forging.

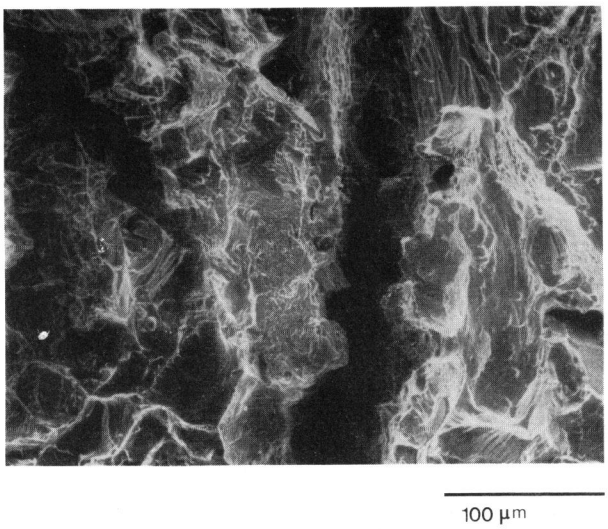

Figure 9 a Scanning electron micrograph of fracture surface of -40°C fracture toughness specimen with high toughness (J_{IC} = 145 N/mm).

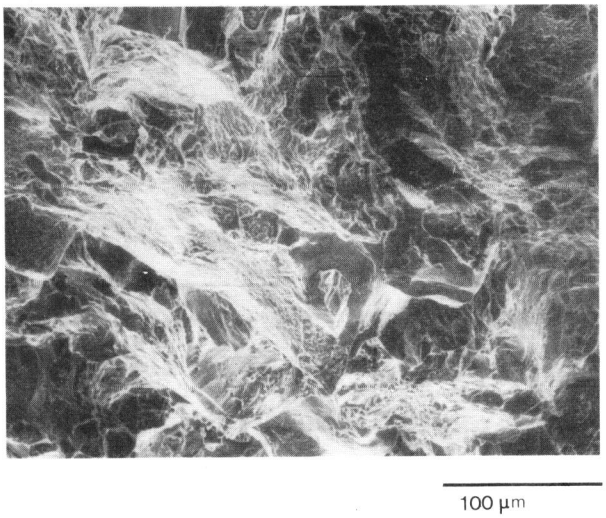

Figure 9 b Scanning electron micrograph of fracture surface of -40°C fracture toughness specimen with low toughness (J_{IC} = 70 N/mm).

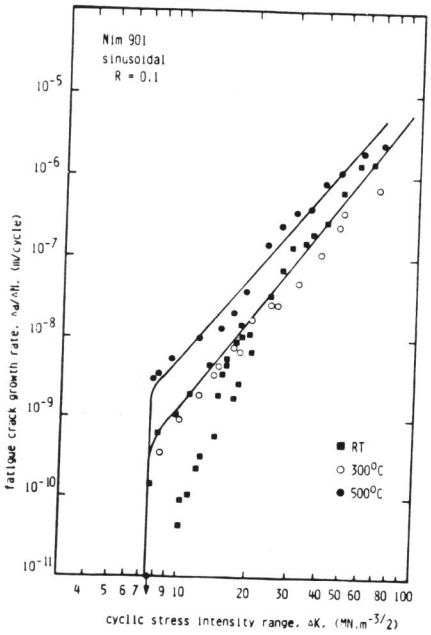

Figure 10 Fatigue crack growth rates of Nim 901 at low mean stress, at different temperatures.

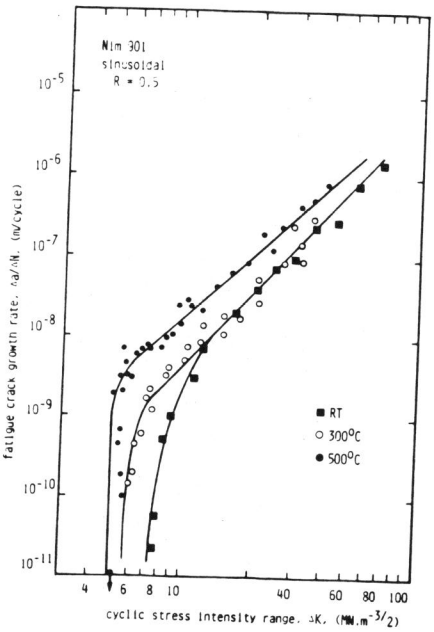

Figure 11 Fatigue crack growth rates of Nim 901 at high mean stress, at different temperatures.

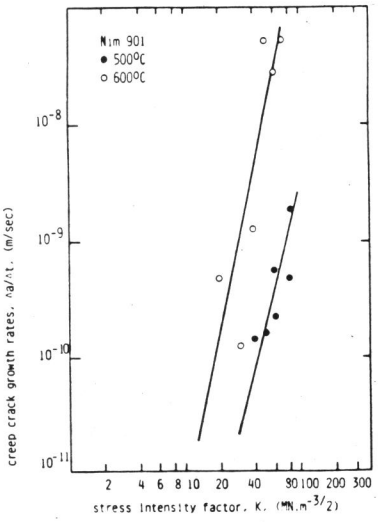

Figure 12 Creep crack growth rates of Nim 901 at different temperatures.

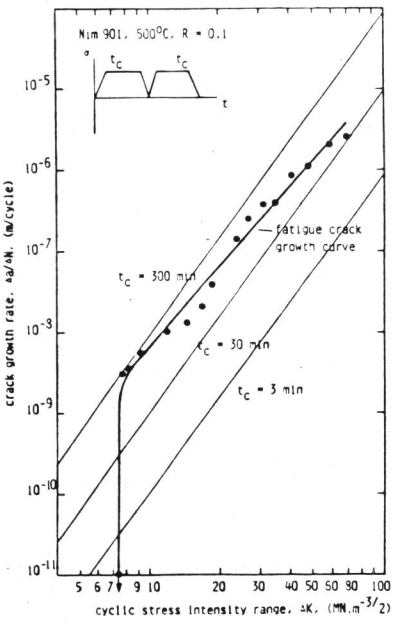

Figure 13 Superposition of creep and fatigue crack growth rates for a trapezoidal load wave shape.